

A Fractional Approach to the Factor Separation Method

SIMON O. KRICHAK AND PINHAS ALPERT

Department of Geophysics and Planetary Sciences, Faculty of Exact Sciences, Tel Aviv University, Tel Aviv, Israel

(Manuscript received 1 August 2001, in final form 2 January 2002)

ABSTRACT

A fractional study of the factor separation (FS) approach is performed. A fractional version of the FS method is discussed. The revised approach allows a determination of role of the acting physical mechanisms as well as that of potential nonlinearity of the modeling system responses. Application of the approach is demonstrated based on the simulations of an eastern Mediterranean weather development during 1–2 November 1994, performed with the Florida State University global spectral model. Thirteen model simulations with varying intensity of the turbulent surface fluxes in the runs were performed for the analysis. Two locations selected for sensitivity analysis of the model results represent the processes over the Red Sea and the Mediterranean Sea. It is shown that the variation of the FS results obtained in the experiments with different intensity of factors may be in some cases significant. The degree of variability of the FS results obtained in the experiments with varying intensity of the factors under the analysis provides useful information on sufficiency (or insufficiency) of available simulation results for an improved evaluation of the role of the acting factors in a meteorological process.

1. Introduction

Atmospheric models are often used as a tool for investigation of the role of different physical processes in atmospheric developments. As was shown by Stein and Alpert (1993, hereafter SA93), such sensitivity analyses may allow determination of not only the contributions of the processes (factors), but also the effects of their synergistic interactions. SA93 suggested a method allowing a determination of the contributions. According to the factor separation (FS) method, the evaluation may be performed based on the model simulations with all possible combinations of the factors switched on/off. The method is widely used; for example, see Alpert and Tsidulko (1994), Alpert et al. (1995a,b), Alpert et al. (1996a,b), Berger (2001); Deleersnijder et al. (1995), Deng and Lilly (1992), Eastman et al. (2001), Guan and Reuter (1996), Khain et al. (1993), Krichak et al. (1997a,b), Ramis and Romero (1995), Romero et al. (1997, 1978), and Reuter and Guan (1995).

In the following we present results of application a modification of the FS method. A revised, fractional approach to the organization of the simulations is discussed. Performing additional model simulations differing from the standard ones by a gradually changing parameter determining the intensity of the factors under analysis is suggested. The results are used for the eval-

uation of the role of hidden potential nonlinearity of the basic system responses.

An example of the application of the approach is presented. The Florida State University Global Spectral Model (FSU GSM; Krishnamurti et al. 1993) was used in the simulation of a case with intensive weather developments during 1–2 November 1994. The case has already been studied using both the large- and mesoscale atmospheric models (Krichak and Alpert 1998; Krichak et al. 2000; Krichak and Levin 2000). The large-scale FSU GSM simulation of the case has provided quite accurate results. Krichak and Alpert (2000) and Krichak and Levin (2000) successfully used the FSU GSM simulation results for organization of the mesoscale downscaling of the development. The analyses allowed selection of the physical factors for the current study. The factors are the surface turbulent sensible and latent heat fluxes. The fact that the FSU GSM accurately simulated the real developments supports an assumption that the large-scale effects of the factors' contributions were also accurately described. An analysis of the role of the effects is presented below.

2. Extended factor separation

A generalization of the FS approach is discussed below. The system of the model equations with both factors excluded may be considered as a base system (BS). When the factors are included, the total time change of the model variable f at a particular point would contain contributions of each factor considered, as well as the contributions due to interactions among the factors. In

Corresponding author address: Dr. Simon O. Krichak, Faculty of Exact Sciences, Department of Geophysics and Planetary Sciences, Tel Aviv University, Ramat Aviv, Tel Aviv 69978, Israel.
E-mail: shimon@cyclone.tau.ac.il

addition, the f time change would also contain contributions of interaction of each factor under analysis with the BS.

Let a and b be two factors (physical effects) under consideration. So if, for instance, a factor is included, then f_{a0} value of f time variation is a result of a joint action of three different effects— \hat{f}_0 contribution of the BS solution, \hat{f}_a contribution of the factor a , and \hat{f}_{a0} contribution of interaction of the hidden BS factors with factor a .

In the case when both a and b factors are under the analysis,

$$f_0 = \hat{f}_0, \tag{1}$$

$$f_{a0} = \hat{f}_0 + \hat{f}_a + \hat{f}_{a0}, \tag{2}$$

$$f_{b0} = \hat{f}_0 + \hat{f}_b + \hat{f}_{b0}, \text{ and} \tag{3}$$

$$f_{ab0} = \hat{f}_0 + \hat{f}_a + \hat{f}_b + \hat{f}_{ab} + \hat{f}_{a0} + \hat{f}_{b0} + \hat{f}_{ab0}. \tag{4}$$

Here,

- f_0 is the time variation of a model characteristic f obtained by integration of the model with the chosen factors a and b excluded (BS);
- f_{a0} is the time variation of a model characteristic f obtained by integration of the model with factor a included;
- f_{b0} is the same, but for of the b factor; and
- f_{ab0} is the same, but when both factors (a and b) are included,

The $|\hat{\psi}|$ terms of the \hat{f}_ψ type represent fractions of f that are contributed by the factor ψ :

- \hat{f}_{a0} is the contribution of interaction of the factor a with the BS;
- \hat{f}_{b0} is the same, but for factor b ;
- \hat{f}_{ab0} is the contribution of joint interaction of the two (a and b) factors with the BS;
- \hat{f}_0 is the pure contribution of the BS solution to the time variation of f ;
- \hat{f}_a is the pure contribution of the factor a to the time variation of f ;
- \hat{f}_b is the same as \hat{f}_a , but for b factor; and
- \hat{f}_{ab} is the pure contribution due to the a and b interaction— a and b synergy.

Solving the system (1)–(4) for the pure contributions ($\hat{f}_0, \hat{f}_a, \hat{f}_b, \hat{f}_{ab}$) yields,

$$\hat{f}_0 = f_0, \tag{5}$$

$$\hat{f}_a = f_{a0} - f_0 - \hat{f}_{a0}, \tag{6}$$

$$\hat{f}_b = f_{b0} - f_0 - \hat{f}_{b0}, \text{ and} \tag{7}$$

$$\hat{f}_{ab} = f_{ab0} - (f_{a0} + f_{b0}) + f_0 - \hat{f}_{ab0}. \tag{8}$$

In many cases the role of the BS-related contributions ($\hat{f}_{a0}, \hat{f}_{b0}, \hat{f}_{ab0}$) may be neglected. This allows using the standard FS formulation as suggested in SA93. In this case, four model simulations are sufficient to evaluate

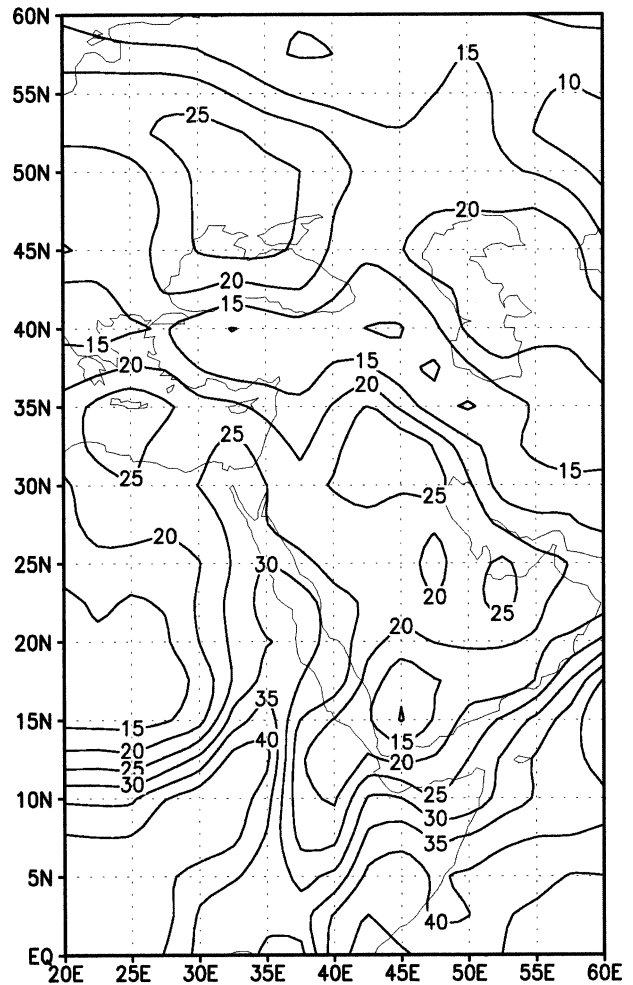


FIG. 1. Precipitable water content, NRP (in $\text{g m}^{-2} \times 10$) for 0000 UTC 1 Nov 1994. Contour interval ($0.5 \text{ g m}^{-2} \times 10$).

the role of two (a and b) chosen factors and that of their synergistic interaction. These are the simulations with a and b factors excluded; a factor excluded, while b is included; a factor is included, but b is excluded; and both a and b are included.

In some cases, however, the role of the ($\hat{f}_{a0}, \hat{f}_{b0}, \hat{f}_{ab0}$) contributions may be significant. Performing additional experiments differing by a varying intensity of the factors under analysis may be used for an evaluation of magnitude of the ($\hat{f}_{a0}, \hat{f}_{b0}, \hat{f}_{ab0}$) contributions. Standard FS-type determination of the contributions of the factors may be performed with the results of each of the simulation sets. Quasi-linear variation in the magnitudes of the contributions obtained in the experiments with linear change of intensity of the factors may be considered an indication to the reliability of results of the standard FS analysis. Conversely, nonlinearity of the model response to the variation of intensity of the factors indicates the significance of the nonlinear responses. Further physical analysis may be required over the areas where such results are obtained.

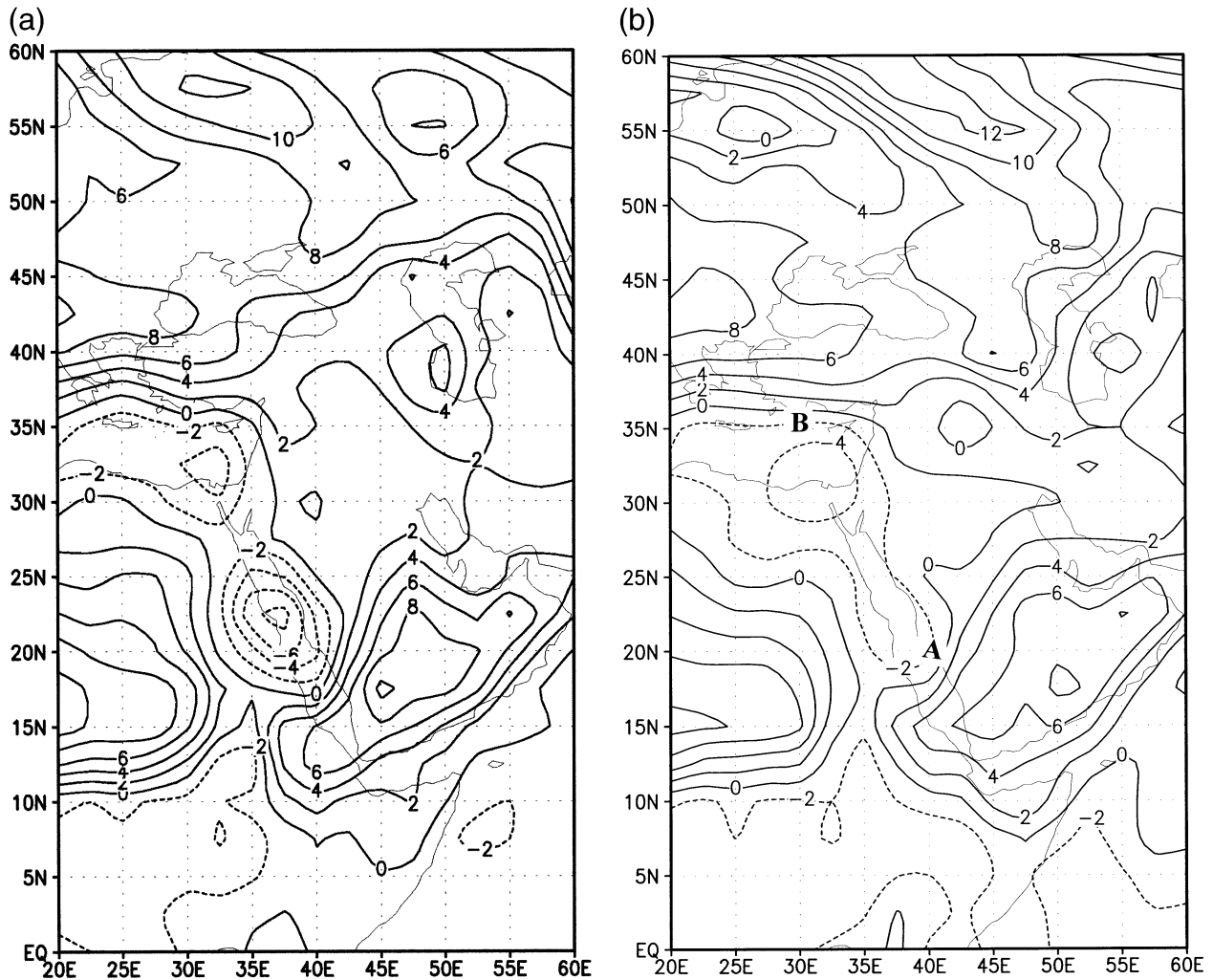


FIG. 2. Best lifted index, NNRP (K). Contour intervals -2 (K). (a) 0000 UTC, (b) 1200 UTC 1 Nov 1994. Indices A, B indicate the locations for Figs. 5 and 6 later.

3. Synoptic description

The following discussion is based on the data from the NCEP–NCAR Reanalysis dataset (NNRP; Kalnay et al. 1996). The NNRP data assimilation system includes the T62/28-level global spectral model with horizontal resolution of about 210 km. The reanalysis data are available with 2.5° lat \times lon horizontal spacing.

The case of 2 November 1994 was characterized by formation of an eastern Mediterranean (EM) cyclone that produced heavy rains in the southern part of the region. Choice of the period for the current analysis has been stimulated by the previous results. A detailed discussion of the synoptic developments and the high-resolution modeling results are available in Krichak and Alpert (1998), Krichak and Levin (2000), and Krichak et al. (2000).

The autumn of 1994 was quite rainy in the Mediterranean region. High positive anomalies of the sea surface temperature (SST) in the Red Sea in October 1994

(up to 3°C ; Reynolds and Smith 1994) suggest that the surface turbulent fluxes could have played a significant role in the unusually intense processes of November 1994. Especially intense weather processes occurred on 2 November 1994 when a cyclone developed causing torrential rains and floods in Egypt and Israel. Unusually intense weather developments were also observed somewhat later (5 November) over other parts of the Mediterranean region (e.g., Lionetti 1996).

NNRP data on the precipitable water content at 0000 UTC and the best lifted stability index (difference between equivalent temperature of a warmest-lifted parcel and the environment temperature; Kalnay et al. 1996) for 0000 UTC and 1200 UTC 1 November 1994 are presented in Figs. 1, 2a, and 2b, respectively. A narrow zone with high moisture content penetrating the Red Sea region may be indicated in Fig. 1. An area with high negative values of the index already existed over the Red Sea and the EM to 0000 UTC on 1 November

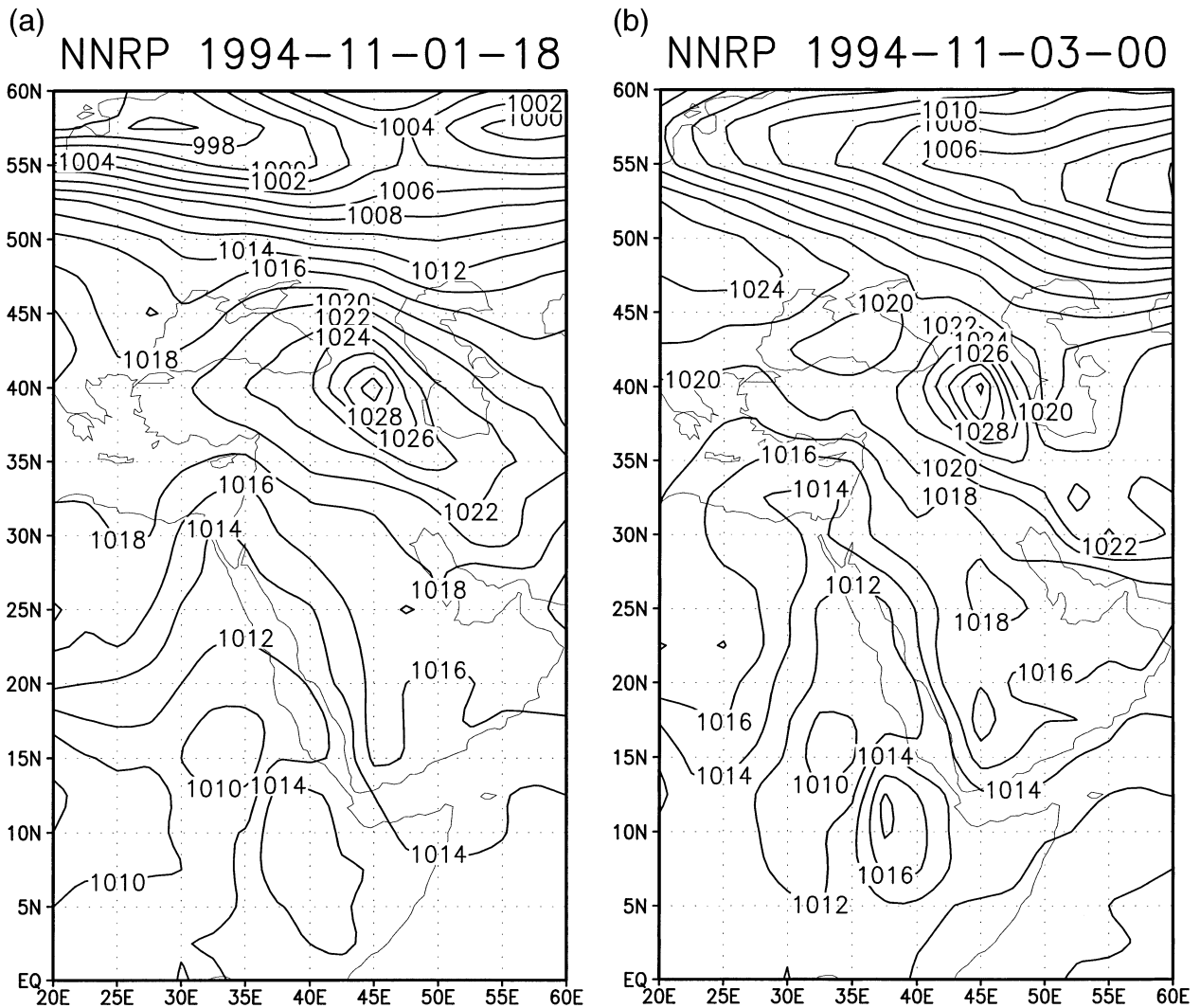


FIG. 3. Sea surface pressure (NNRP) for (a) 1800 UTC 1 Nov and (b) 0000 UTC 3 Nov 1994 (contour interval -2 hPa).

1994, that is, prior to the cyclone development (Fig. 2a). The index value was especially low (-8) over the Red Sea. This indicated a high level of instability of the air mass over the area. The instability zone was rapidly shifting to the north. On the pattern corresponding to 1200 UTC 1 November 1994 the area was already located over the EM (Fig. 2b). NNRP sea level pressure patterns (SLP) for 1800 UTC 1 November and 0000 UTC 3 November 1994 are presented in Figs. 3a and 3b respectively. No EM cyclone was found in Fig. 3a (1800 UTC 1 November 1994). The cyclone already existed in the pattern for 0000 UTC 3 November 3 (Fig. 3b). Southward propagation of a trough zone over Caspian Sea, insignificant (about $1-2$ hPa) growth of the SLP over the Red Sea, and minor variations of the SLP over the equatorial Arabian Sea may also be indicated.

The unusual intensity of the synoptic processes has been associated with the transport of huge amounts of warm and moist air masses to the EM from the Red Sea

and the Arabian Sea area to 0000 UTC 1 November 1994 (Krichak and Alpert 1998). Formation of a mid-latitude Red Sea Trough (RST) cyclone (Krichak et al. 1997a,b) took place. According to Krichak and Alpert (2000) the RST intensification may partly be attributed to the role of the surface turbulent heat [sensible heat flux (SHF)] and moisture [latent heat flux (LHF)] exchanges due to the unusually high SST anomaly in the Red Sea area.

4. The model and organization of the simulations

The FSU GSM (Krishnamurti et al. 1993) was adapted. The hydrostatic FSU GSM (Krishnamurti et al. 1993) has the following main characteristics:

- independent variables ($x, y, \sigma-p, t$); and
- dependent variables (vorticity, divergence, surface pressure, vertical velocity, temperature, and humidity).

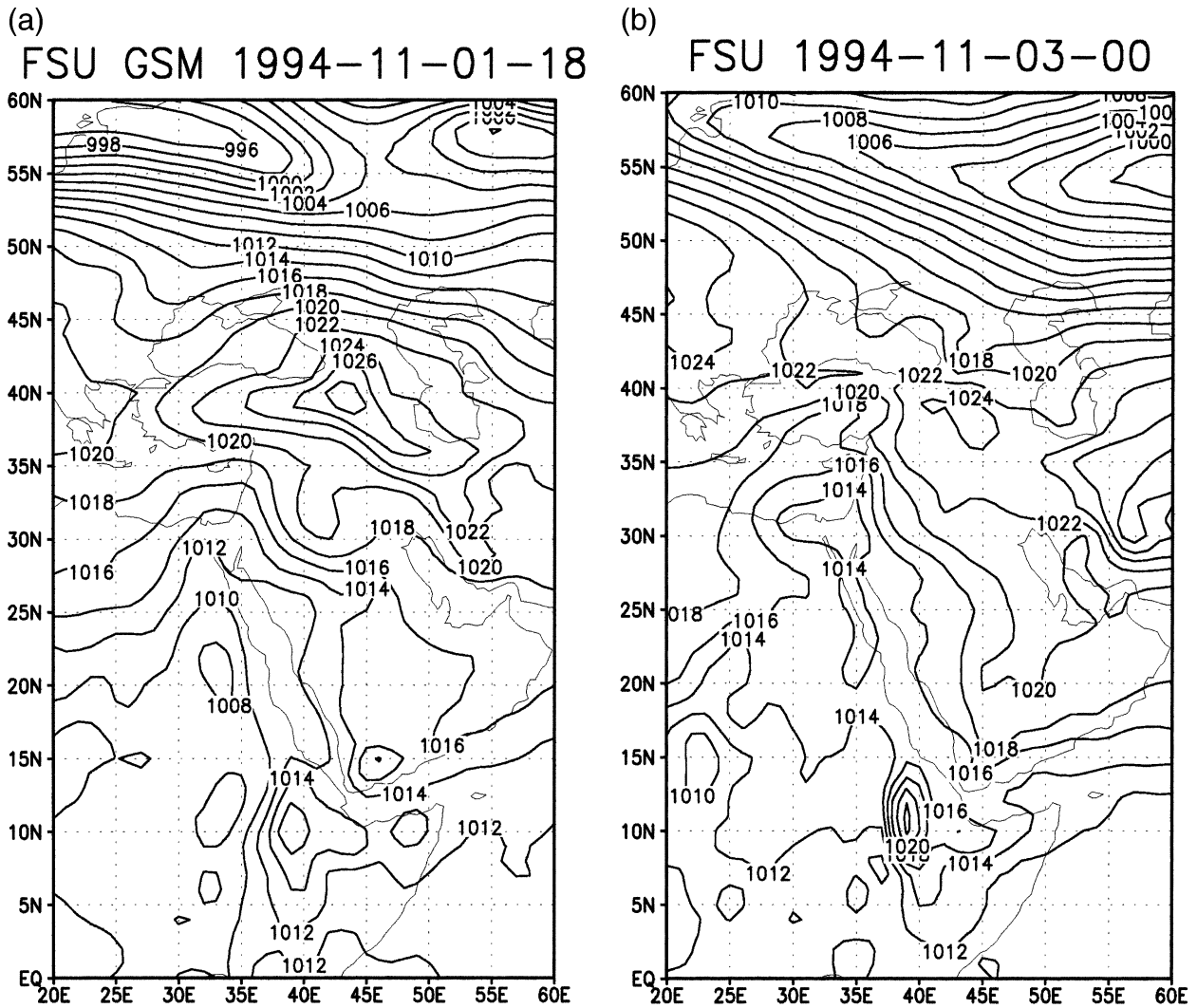


FIG. 4. Same as in Fig. 3, but for the FSU GSM forecasts started from 1200 UTC 1 Nov 1994 (contour interval 2 hPa).

T106 spectral horizontal truncation (equivalent to about 100-km resolution) is adapted. The atmosphere in the model has 14 layers between roughly 50 and 1000 hPa, with four levels in the boundary layer. A semiimplicit time difference scheme is used. An explicit time difference scheme is applied (slow modes). For handling the fast modes, the implicit approach is adapted; envelope topography is used; a centered vertical difference scheme is adapted for all variables except for humidity, which is handled by an upstream scheme (energy conserving); and fourth-order horizontal diffusion used.

Kuo-type cumulus parameterization, shallow convection, dry convective adjustment, and large-scale condensation parameterization schemes are adapted. Surface fluxes are computed via the similarity theory. Vertical distribution of fluxes is determined utilizing the diffusive formulation. Computation of long- and short-wave radiative fluxes is performed based on a band model. Parameterization of low, middle, and high clouds

is based on threshold-relative humidity for radiative transfer calculations. Surface energy balance is coupled to the similarity theory.

Global simulations were initiated at 1200 UTC 1 November 1994 and continued for 36 h. The initial data for the simulations were adapted from the European Center for Medium-Range Weather Forecasts' (ECMWF) objective analyses data archive. The use of the ECMWF and not the NNRP analyses is due to a higher horizontal resolution of the ECMWF data. The data are globally determined at 13 surfaces (1000, 925, 850, 700, 500, 400, 300, 250, 200, 150, 100, 70, and 50 hPa) with 1.15° horizontal resolution.

The model results were available for analysis on latitude-longitude grid with 1° × 1° resolution. Results of the model simulation of the SLP developments on the area are presented in Figs. 4a and 4b for 1800 UTC 1 November and 0000 UTC 3 November 1994, respectively. The corresponding NNRP patterns are available

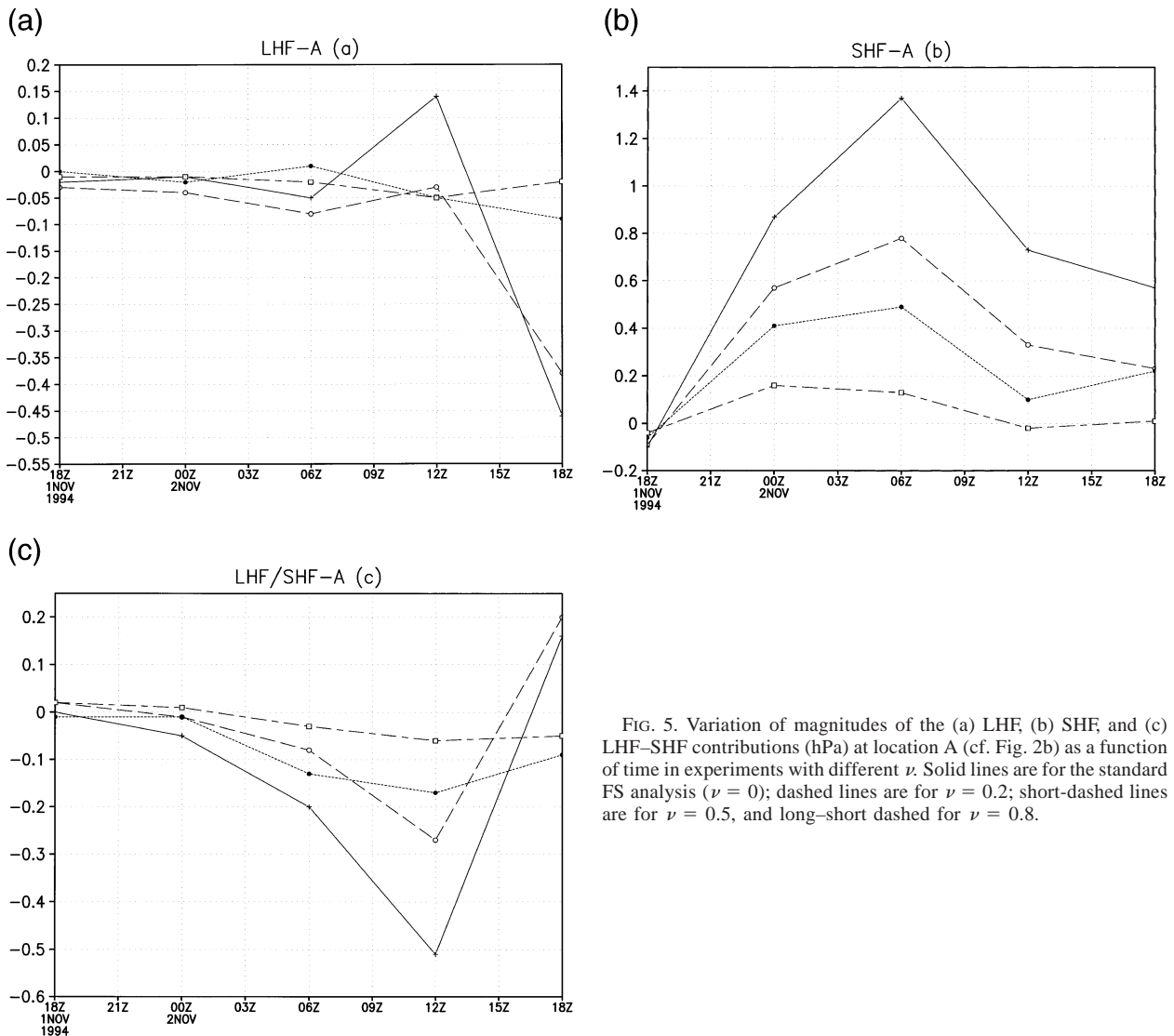


FIG. 5. Variation of magnitudes of the (a) LHF, (b) SHF, and (c) LHF–SHF contributions (hPa) at location A (cf. Fig. 2b) as a function of time in experiments with different ν . Solid lines are for the standard FS analysis ($\nu = 0$); dashed lines are for $\nu = 0.2$; short-dashed lines are for $\nu = 0.5$, and long–short dashed for $\nu = 0.8$.

for the verification in Figs. 3a and 3b. The real large-scale developments are quite accurately described in the model simulation.

Factor separation analysis of the SLP simulation for the period from 1800 UTC 1 November until 1800 UTC 2 November 1994 was performed. Additional parameter ν was introduced in the model formulation. The parameter determines intensity of the factors under the analysis. It is assumed that the same ν value may be used for both a and b factors. In this case, the LHF and/or SHF are fully included in the control run simulation when $\nu = 1$. The standard FS case with total exclusion of the factors occurs when $\nu = 0$. Partial exclusion of any factor is achieved with $0 < \nu < 1$.

Thirteen model simulations of the synoptic development were performed. They consisted of one simulation with the both (LHF and SHF) factors included (control run) and four three-run simulation sets using

different values of ν . The linearly varying (rounded off) values of ν were chosen. In the first group of experiments, $\nu = 0.8$ was used; the second group, $\nu = 0.5$; the third group, $\nu = 0.2$; and the fourth group, $\nu = 0$ (BS, in case the both factors are excluded). The fourth group corresponded to the standard FS formulation; in the other three groups ν values characterized some degree of exclusion of the factors. Results of experiments of the first group were expected to differ only slightly from those of the control run. The differences with the control run are expected to become larger for the second and third groups and to maximize in the fourth group of simulations.

5. Results

Factor separation computations were performed for two locations representing different areas of the pro-

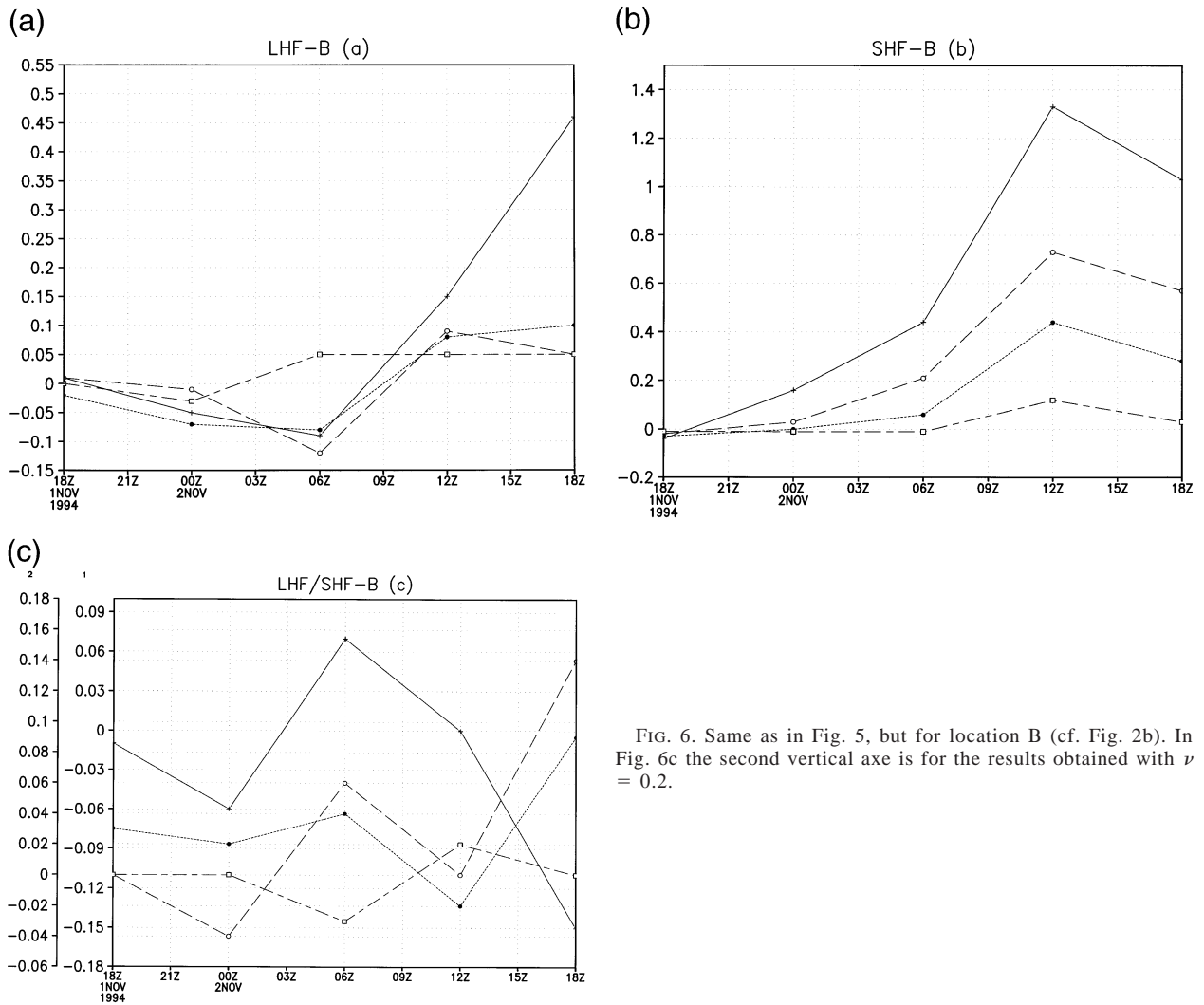


FIG. 6. Same as in Fig. 5, but for location B (cf. Fig. 2b). In Fig. 6c the second vertical axis is for the results obtained with $\nu = 0.2$.

cess development. The points are positioned over the Red Sea (A) and eastern Mediterranean (B), respectively (Fig. 2b). Results of the FS computation of LHF, SHF, and the LHF–SHF (i.e., synergy) contributions in each of the simulation sets are presented in Figs. 5 and 6a–c, for locations A and B, respectively. Here, solid lines represent results of the standard FS analysis ($\nu = 0$); dashed lines represent runs with $\nu = 0.2$;

short-dashed lines have $\nu = 0.5$, and long–short-dashed are $\nu = 0.8$.

Results of the FS analysis for point A over the Red Sea (20°N, 40°E) are presented in Figs 5a–c. The behavior of the graphs corresponding to the different values of ν is quite consistent here in the case of the SHF factor (Fig. 5b). The factor was contributing to the observed SLP increase during the period (max equal

TABLE 1. Correlation of the contributions computed in three experiment groups with varying ν with those of the standard FS. First group has $\nu = 0.8$; second group has $\nu = 0.5$; third group has $\nu = 0.2$; fourth group has $\nu = 0.0$ (standard FS).

Time (h)	Group III vs IV			Group II vs IV			Group I vs IV		
	LHF	SHF	Synergy	LHF	SHF	Synergy	SHF	LHF	Synergy
6	0.97	0.98	0.99	0.94	0.93	0.96	0.93	0.72	0.84
12	0.95	0.98	0.98	0.90	0.94	0.93	0.74	0.81	0.79
24	0.93	0.93	0.97	0.87	0.91	0.91	0.68	0.83	0.72
36	0.92	0.97	0.96	0.85	0.93	0.89	0.64	0.79	0.63
48	0.94	0.96	0.96	0.86	0.92	0.91	0.61	0.71	0.68

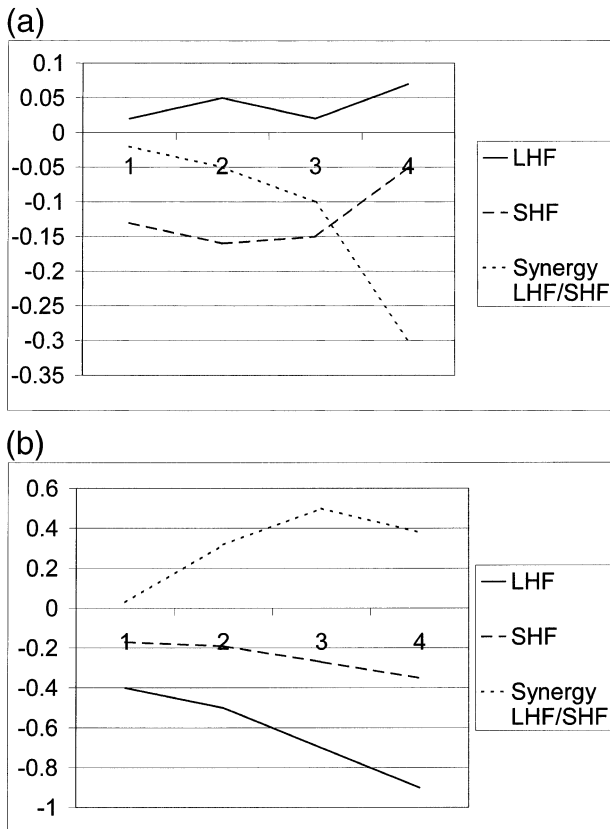


FIG. 7. Variation of magnitudes of the LHF, SHF, and LHF-SHF contributions at a location over the Arabian Sea as a function of ν computed separately for (a) 12-h and (b) 24-h forecast results. The numbers 1-4 indicate results obtained for $\nu = 0.8, 0.5, 0.2, 0.0$, respectively.

to 1.4 hPa, Fig. 5b). The role of the LHF was neutral until 0900 UTC, when the FS results demonstrate a cyclogenetic contribution of the factor (Fig. 5a). This FS result is not fully reliable—behavior of the curves for the different simulation sets is not consistent. Results of the FS determination of the SHF-LHF synergistic factor are quite consistent in the fractional FS experiments. The cyclogenetic contribution of the interaction term was increasing almost until the end of the simulation period (Fig. 5c). The role of the effect was however quite small. According to the results, the observed developments over the EM were influenced by the total cyclolitic effect of the surface turbulent heat fluxes over the Red Sea area. The effect contributed to the northward propagation of the unstable air masses.

Location B (35°N, 30°E) represented the EM region where the intensive cyclogenetic process occurred. The FS results for the SHF factor (Fig. 6b) consistently demonstrate its strong (up to 1.4 hPa) cyclolitic role in the process during the simulation period. The result could be expected: not the local EM effects played the main role in the development. Fractional FS tests of

the LHF contributions (Fig. 6a) reveal a minor cyclogenetic contribution of the LHF factor until 0000 UTC-0600 UTC 2 November (Fig. 6a). The FS results become less reliable after 0000 UTC 2 November. Still, the obtained results demonstrate a cyclolitic role of the LHF factor after 0600 UTC at the location. Variation of the corresponding graphs representing the role of the synergistic interaction is available in Fig. 6c [the second vertical axis corresponds to the results obtained with $\nu = 0.2$ (dashed lines)]. Behavior of the graphs in the figure is quite inconsistent, especially after the first 9-12 h of the 24-h run. The low level of consistency demonstrates a lack of reliability of the FS results in this case. The result may also mean that the synergistic factor was not among the main effects responsible for the EM cyclogenesis.

The nonlinear variation in the magnitudes of the contributions with linear change of ν was considered here as an indication that additional (hidden) interactions (or instability) play a significant role. Further physical analysis may be required in such cases. Application of the considerations is additionally illustrated by Figs. 7a and 7b. Contributions of the three factors (in hPa, LHF, SHF, and LHF-SHF) over a location in the tropical area of the Arabian Sea (5°N, 55°E) are presented here as a function of ν for the forecasts to 12 and 24 h, respectively. The SHF, LHF, and SHF-LHF contributions here are varied nonlinearly with the linear variation of ν (not presented). Variation of magnitudes of the LHF, SHF, and LHF-SHF contributions in the area as a function of ν separately computed for 12 and 24 h forecast results are presented in Figs. 7a and 7b respectively. Numbers 1-4 in the figures indicate results obtained for $\nu = 0.8, 0.5, 0.2, 0.0$, respectively. Behavior of the graphs in Fig. 7a (12-h forecast) is nonlinear for all the factors considered. The situation is different in Fig. 7b, corresponding to the 24-h forecast. Here graphs vary quite linearly with the ν variation. The FS results based on the 24-h forecast data over the location representing the tropical area of the Arabian Sea appear to be more reliable than those of the 12-h forecast.

The patterns discussed (Figs. 5 and 6) characterize the FS results at two locations only. Additional understanding on the validity of the FS results over the whole domain can be obtained with the help of the map correlation analysis. Correlation coefficients r between contributions of factors computed in the experiments with different values of ν over the area 0°-35°N, 0°-60°E are presented in Table 1:

$$r = \frac{\sum_{i=1}^N [(X_1)_i - \bar{X}_1][(X_2)_i - \bar{X}_2]}{N\sigma_1\sigma_2}. \quad (9)$$

Here, indices $k = 1, 2$; X is the contributions of the factors under consideration at the model grids points; N is total number of points in the array and

$$\sigma_k = \sqrt{\frac{\sum_{i=1}^N [(X_k)_i - \bar{X}_k]^2}{N}}; \quad \bar{X}_k = \frac{1}{N} \sum_{i=1}^N X_i. \quad (10)$$

Comparison of the values in Table 1 allows an integrated evaluation of the FS results over the area. A sufficient level of the reliability can be expected when results of at least two sets of FS simulations with different intensities of the acting factors produce consistent results. Over the whole area, the condition was not fully fulfilled. The FS estimations based on results of the third and the fourth groups of simulations are well correlated. The correlations are lower in the case of the second through fourth groups. The correlations between the FS estimates based on results of the first and fourth groups are even lower. The level of the correlation also decreases with the forecast time. The result is not unexpected. It illustrates the importance of accurate model representation of a process under analysis for application of the FS approach.

6. Summary

Results of a fractional sensitivity analysis of the FS method are presented and discussed. Application of the fractional approach is exemplified with a case of an intensive trough development over the EM region. It is shown that the variation of the FS results obtained in the experiments with different intensity of factors may be, in some cases, significant. It is not unexpected to find that the fractional FS results on the average become less consistent with time. For example, for $\nu = 0.8$ the map correlation of the contributions of SHF dropped from 0.93 at a 6-h simulation to 0.61 at a 48-h run.

The degree of variability of the FS results obtained in the experiments with varying intensity of the factors under the analysis provides a useful information on sufficiency (or insufficiency) of available simulation results for an improved evaluation of the role of the acting factors in a meteorological process.

Acknowledgments. This work was supported by the Binational US–Israel Science Foundation (BSF) Grant 97-00448 and Israeli Ministry of Science Grants 6934-96 and 9470-98. ECMWF objective analysis data for 1200 UTC 1994 were used in the simulations. Initial processing of the data was performed at the Florida State University in the process of work on the BSF-supported project (Grant 92-00275). Adaptation of the FSU GSM model at Tel Aviv University (TAU) was performed as a part of the work on the project. Computations were performed on the Cray J932 computer, Israeli Inter-University Computing Center.

The authors thank R. Borshtein for his comments on the manuscript. We would also like to extend our gratitude to T. N. Krishnamurti for providing the FSU GSM model for adaptation at TAU. One of the authors (SK) thanks V. A. Gordin for the fruitful discussion. Finally, we appreciate the constructive remarks by the reviewers.

NCEP Reanalysis data provided by the NOAA–CIRES Climate Diagnostics Center, Boulder, Colorado, from their Web site at <http://www.cdc.noaa.gov/>, were used in the study.

REFERENCES

- Alpert, P., and M. Tsidulko, 1994: Project WIND—Numerical simulations with Tel-Aviv PSU/NCAR model at Tel-Aviv University 1994. *Mesoscale Modelling of the Atmosphere, Meteor. Monogr.*, No. 25, Amer. Meteor. Soc., 81–95.
- , U. Stein, and M. Tsidulko, 1995a: Role of sea fluxes and topography in eastern Mediterranean cyclogenesis. *The Global Atmosphere–Ocean System*, Vol. 3, 55–79.
- , M. Tsidulko, and U. Stein, 1995b: Can sensitivity studies yield absolute comparisons for the effects of several processes? *J. Atmos. Sci.*, **52**, 597–601.
- , S. O. Krichak, T. N. Krishnamurti, U. Stein, and M. Tsidulko, 1996a: The relative roles of lateral boundaries, initial conditions, and topography in mesoscale simulations of lee cyclogenesis. *J. Appl. Meteor.*, **35**, 1091–1099.
- , M. Tsidulko, S. O. Krichak, and U. Stein, 1996b: A multi-stage evolution of an ALPEX cyclone. *Tellus*, **48A**, 209–220.
- Berger, A., 2001: The role of CO₂, sea level and vegetation during Milankovitch-forced glacial-interglacial cycles. *Geosphere–Biosphere Interactions and Climate*, L. Bengtsson and C. U. Hammer, Eds., Cambridge University Press, 318 pp.
- Deleersnijder, E., J. Ozer, and B. Tartinville, 1995: A methodology for model intercomparison: Preliminary results. *Ocean Model.*, **107**, 6–9.
- Deng, L., and D. K. Lilly, 1992: Helicity effect on turbulent decay in a rotating frame. Preprints, *10th Symp. on Turbulence and Diffusion*, Portland, OR, Amer. Meteor. Soc., 338–341.
- Eastman, J. L., M. B. Coughenour, and R. A. Pilke, 2001: The effects of CO₂ and landscape change using a coupled plant and meteorological model. *Global Change Biol.*, in press.
- Guan, S., and G. W. Reuter, 1996: Numerical simulation of an industrial cumulus affected by heat, moisture and CCN released from an oil refinery. *J. Appl. Meteor.*, **35**, 1257–1264.
- Kalnay, E., and Coauthors, 1996: The NCEP/NCAR 40-Year Reanalysis Project. *Bull. Amer. Meteor. Soc.*, **77**, 437–471.
- Khain, A. P., D. Rosenfeld, and I. Sednev, 1993: Coastal effects in the E. Mediterranean as seen from experiments using a cloud ensemble model with detailed description of warm and ice microphysical processes. *Atmos. Res.*, **30**, 295–319.
- Krichak, S. O., and P. Alpert, 1998: Role of large-scale moist dynamics in November 1–5, 1994 hazardous Mediterranean weather. *J. Geophys. Res.*, **103**, 19 453–19 458.
- , and Z. Levin, 2000: On the cloud microphysical processes during the November 2, 1994, hazardous storm in the southeastern Mediterranean as simulated with mesoscale model. *Atmos. Res.*, **53**, 63–89.
- , P. Alpert, and T. N. Krishnamurti, 1997a: Interaction of topography and tropospheric flow—A possible generator for the Red Sea trough? *Meteor. Atmos. Phys.*, **63**, 149–158.
- , —, and —, 1997b: Red Sea trough/cyclone development numerical investigation. *Meteor. Atmos. Phys.*, **63**, 159–170.
- , M. Tsidulko, and P. Alpert, 2000: November 2, 1994 severe storms in the southeastern Mediterranean. *Atmos. Res.*, **53**, 45–62.
- Krishnamurti, T. N., H. S. Bedi, and K. Ingles, 1993: Physical initialization using SSM/I rain rates. *Tellus*, **A45**, 247–269.
- Lionetti, M., 1996: The Italian floods of the 4–6 November 1994. *Weather*, **51**, 18–27.
- Ramis, S., and R. Romero, 1995: A first numerical simulation of the development and structure of the sea breeze in the Island of Mallorca. *Ann. Geophys.*, **13**, 981–994.
- Reuter, G. W., and S. Guan, 1995: Effects of industrial pollution on cumulus convection and rain showers: A numerical study. *Atmos. Environ.*, **29**, 2467–2474.

- Reynolds, R. W., and T. M. Smith, 1994: Improved global sea surface temperature analysis. *J. Climate*, **7**, 929–948.
- Romero, R., C. Ramis, and S. Alonso, 1997: Numerical simulation of an extreme rainfall event in Catalonia: Role of orography and evaporation from the sea. *Quart. J. Roy. Meteor. Soc.*, **123**, 537–559.
- , ———, ———, C. A. Doswell III, and D. J. Stensrud, 1998: Mesoscale model simulations of three heavy precipitation events in the western Mediterranean region. *Mon. Wea. Rev.*, **126**, 1859–1881.
- Stein, U., and P. Alpert, 1993: Factor separation in numerical simulations. *J. Atmos. Sci.*, **50**, 2107–2115.